

Tip of the Red Giant Branch Bounds on the Neutrino Magnetic Dipole Moment Revisited

Noah Franz 

*Institute for Astronomy, University of Hawai‘i, 2680 Woodlawn Drive, Honolulu, HI 96822, USA and
Department of Physics and Astronomy, Siena College, 515 Loudon Rd, Loudonville, NY 12211, USA*

Mitchell Dennis 

Institute for Astronomy, University of Hawai‘i, 2680 Woodlawn Drive, Honolulu, HI 96822, USA

Jeremy Sakstein 

Department of Physics and Astronomy, University of Hawai‘i, Watanabe Hall, 2505 Correa Road, Honolulu, HI 96822, USA

(Dated: July 26, 2023)

We use a novel method to constrain the neutrino magnetic dipole moment (μ_ν) using the empirically-calibrated tip of the red giant branch I-band magnitude that fully accounts for uncertainties in stellar physics. Our method uses machine learning to emulate the results of stellar evolution codes. This reduces the I-Band magnitude computation time to milliseconds, which enables a Bayesian statistical analysis where μ_ν is varied simultaneously with the stellar physics, allowing for a complete exploration of parameter space. We find the region $\mu_\nu \leq 6 \times 10^{-12} \mu_B$ (with μ_B the Bohr magneton), previously believed to be excluded, is unconstrained after accounting for degeneracies with stellar physics. It is likely that larger values are similarly unconstrained. We discuss the implications of our results for future neutrino magnetic dipole moment searches and for other astrophysical probes.

I. INTRODUCTION

The high temperatures and densities in the cores of stars makes them naturally occurring laboratories that allow astronomers to probe the properties of light ($< 10\text{keV}$), weakly interacting particles (e.g., [1, 2]). Examples of theories that can be probed using these stellar laboratories are those that include axions [3–5], hidden photons [6], and a larger neutrino magnetic dipole moment (MDM) than predicted by the Standard Model of Particle Physics (SM) [7, 8]. Unlike terrestrial laboratories, stellar interiors are subject to large uncertainties due to environmental variations (e.g., mass and metallicity) and uncertain input physics e.g., mixing length, opacity, and nuclear reaction rates. Any attempt to bound new physics using these objects should simultaneously vary the stellar physics parameters to incorporate their effects (including degeneracies) into the final uncertainty. Unfortunately, the long run-times of stellar structure codes (\sim hours or longer) prevents the use of Bayesian statistical methods such as Markov Chain Monte Carlo (MCMC) sampling, which require run-times of order seconds or shorter. For this reason, previous works have either held the stellar physics fixed or varied parameters individually with all others held fixed.

Recently, two of us presented a novel method that enables MCMC analyses of stellar observations to constrain stellar input physics [9] and the axion-electron coupling [10]. This method trains a machine learning emulator to predict stellar observables as a function of the stellar and beyond SM physics parameters. The emulator, which evaluates in milliseconds, is called by the MCMC sampler at each point in parameter space rather than a stellar structure code, allowing for rapid con-

vergence. Applying this method to tip of the red giant branch (TRGB) bounds on the axion-electron coupling revealed that the range $0 \leq \alpha_{26} \leq 2$, previously believed to be excluded, is unconstrained once the degeneracies between stellar parameters are accounted for [10]. In this work, we apply this method to reevaluate TRGB bounds on the neutrino MDM, which affects stars in a similar manner to light axions. The SM predicts a neutrino MDM $\mu_\nu = 3.20 \times 10^{-19} \mu_B$, where $\mu_B = e/2m_e$ is the Bohr Magnetron [2, 11, 12]; too small to effect stellar evolution. In contrast, some extensions of the SM predict neutrino MDMs that are larger by several orders of magnitude [13]. By constraining the neutrino MDM we can therefore eliminate extensions of the SM.

TRGB stars provide the most stringent constraints on the neutrino MDM [14]. Low-mass stars ($M \lesssim 2.25M_\odot$ depending on metallicity and other parameters) enter this stage of evolution after reaching a core temperature of $\approx 10^8\text{K}$ in a degenerate helium core surrounded by a hydrogen burning shell. At this temperature, a runaway helium reaction creates an explosion resulting in the *helium flash*. The star rapidly moves to the horizontal branch, leaving a visible discontinuity in the color-magnitude diagram — the TRGB. The TRGB consistency across parameter space (e.g. initial helium abundance, initial metallicity) in the I-band magnitude, M_I^{TRGB} , makes it useful as a standard candle [15–19]. M_I^{TRGB} and its uncertainty are calculated either by calibrating observational data [14, 20] or by calculating it theoretically using stellar structure codes [21, 22]. The error on the observational calibration of M_I^{TRGB} is smaller than that on the theoretical calculation because of uncertainties in the stellar input physics

[21, 22] and large empirical errors on the bolometric corrections needed to convert the outputs of stellar structure codes to magnitudes. For this reason, observational calibration of M_I^{TRGB} is the standard in the literature.

A larger neutrino MDM than predicted by the SM causes additional energy losses in the plasma and pair-production channels [23] that decrease the core temperature. In turn, the hydrogen shell burning phase is lengthened, and more helium is deposited on the core, resulting in a more energetic explosion and consequentially a brighter Helium flash [14, 24, 25]. Many works have used this effect to constrain the neutrino MDM by comparing empirical calibrations of M_I^{TRGB} with the results of incorporating the additional energy losses due to a large MDM into stellar structure codes [2, 14, 23, 25, 26]. Most recently, [14] obtained the most restrictive limit: $\mu_\nu < 1.2 \times 10^{-12} \mu_B$ at the 95% confidence level using calibrated observations of ω -Centauri. In this work, we reanalyze the calibrations studied by [14] using our MCMC-machine learning method to account for degeneracies with the mass, metallicity, and initial helium abundance, and find that the region $\mu_\nu \leq 6 \times 10^{-12} \mu_B$ is unconstrained once these degeneracies are accounted for.

This paper is organized as follows: §II outlines the methodology we implement to constrain the neutrino MDM including subsections on the modification of the stellar evolution code, our machine learning emulator, and our MCMC analysis. §III presents and discusses the results of the stellar evolution code modifications, the machine learning emulator, and the MCMC analysis. §IV discusses the implications of our results, examines the limitations of our methodology, and suggests future work. We conclude in §V.

All of the codes used in this work including our MESA inlists, modifications, and output files; machine learning emulators; and MCMC scripts are available in a reproduction package at the following URL: <https://doi.org/10.5281/zenodo.8173321> [27].

II. METHOD

A. Stellar Evolution Code and Training Set

We modified the stellar evolution code MESA version 12778 [28–33] to add an extra component to the SM neutrino energy loss, giving a total loss rate per unit mass:

$$\varepsilon_{\text{tot}} = \varepsilon_{\text{plasma}}^\mu + \varepsilon_{\text{pair}}^\mu + \varepsilon_{\text{SM}}, \quad (1)$$

where ε_{tot} is the energy loss per unit mass, ε_{SM} is the SM energy loss rate calculated by MESA, $\varepsilon_{\text{plasma}}^\mu$ is the plasma energy loss rate due to neutrino MDM given by [23, 34],

$$\varepsilon_{\text{plasma}}^\mu = 0.318 \varepsilon_{\text{plasma}} \left(\frac{10 \text{ keV}}{\omega_{\text{plasma}}} \right)^2 \mu_{12}^2, \quad (2)$$

and $\varepsilon_{\text{pair}}$ is the pair production energy loss rate due to neutrino MDM given by [23],

$$\varepsilon_{\text{pair}}^\mu = 1.6 \times 10^{11} \text{ erg g}^{-1} \text{ s}^{-1} \times \frac{\mu_{10}^2}{\rho_4} e^{-118.5/T_8}. \quad (3)$$

In equation (2), $\varepsilon_{\text{plasma}}$ is the SM plasma energy loss rate, $\mu_{12} = \mu_\nu/10^{12} \mu_B$, where μ_ν is the neutrino MDM, and ω_{plasma} is given by,

$$\omega_{\text{plasma}}^2 = \frac{4\pi\alpha n_e}{m_e}, \quad (4)$$

where α is the fine-structure constant, n_e is the electron number density, and m_e is the mass of an electron. In equation (3), $\mu_{10} = \mu_\nu/10^{10} \mu_B$, $\rho_4 = \rho/10^4 \text{ g cm}^{-3}$ where ρ is the density, and $T_8 = T/10^8 \text{ K}$ where T is the temperature.

In order to directly compare our simulated results with observations, we must convert from MESA output quantities to M_I^{TRGB} . Furthermore, the empirical calibration of M_I^{TRGB} has a strong $(V - I)$ color dependence. Any particular MESA model could have a final $(V - I)$ which differs from the reference $(V - I)$ color (zero-point) of the given calibration. It is therefore necessary to use a color-correction to shift the model output (both $(V - I)$ and M_I^{TRGB}) to the reference color. The color dependence of each system is unique, leading to different color-corrections for each system. We used the empirical bolometric corrections of Worthey & Lee (WL) [35] to make this conversion. WL takes the surface gravity, $[\text{Fe}/\text{H}]$, luminosity, and effective temperature from the MESA models and calculates bolometric corrections used to calculate the I-band magnitude, $(V - I)$ color, and both the empirical I-band and $(V - I)$ color errors. These were then passed into the color-correction of the form $M_I^{\text{TRGB}} = f(M_I, (V - I))$ given in Table I. The procedure above is tantamount to assuming that the TRGB I-band magnitude is due solely to the brightest star. Whereas this is a reasonable first-approximation [36], we discuss how one could use our ML emulator to make a more realistic theoretical prediction in §IV D. The purpose of our present study is to compare with previous bounds on μ_ν , which make the same single-star approximation [36, 37], so adopting this approximation ensures that our conclusions are driven by uncertainties and degeneracies in the stellar modeling parameters and not by difference in the theoretical prescriptions.

Using the modified version of MESA and the WL conversion, we ran a grid of 146,250 MESA models from the pre-main-sequence to the TRGB (defined as the point where the power in helium burning exceeds 10^6 ergs/s) with varying stellar mass (M), metallicity (Z), initial helium fraction (Y), and neutrino MDM (μ_{12}). The grid includes input ranges of $0.7 \leq M/M_\odot \leq 2.25$, $0.2 \leq Y \leq 0.3$, $10^{-5} \leq Z \leq 0.04$, and $0 \leq \mu_{12} \leq 6$. The range of M , Y , and Z covers the range where a core helium flash is expected [38], and the range of μ_{12} covers values where M_I^{TRGB} does not differ from the SM prediction to values where main-sequence stars begin to be affected. The

ranges of M , Y , and Z were chosen to be larger than the range where a core helium flash is expected in order to account for the possibility that including a neutrino MDM could cause a core flash in models that would not contribute to the TRGB in the SM, and to ensure that the boundary between a core flash and stable helium burning is resolved. As we will discuss shortly, this is essential for ensuring accurate emulation. We used 15, 10, 25, and 38 points for M , Y , Z , and μ_{12} respectively. The spacing in M and Y was linear and the spacing in Z and μ_{12} was logarithmic. The training data was generated uniformly across parameter space (either linearly or logarithmically); however we note that as the dimensionality of the parameter space increases, more efficient sampling methods such as Latin hypercube sampling will be necessary. Due to limited computation time, we did not vary other parameters predicted to have an effect on the brightness of the TRGB such as mixing length, mass loss, opacity, and neutrino loss rate [21, 22]. Simultaneously varying these parameters can only add more uncertainties and can therefore only strengthen our conclusions. All MESA parameters that we hold constant assume identical values to those in [39], with the exception of the mixing length, which was set to $\alpha_{MLT} = 2.0$. The precise choices we made for these parameters can be found in the MESA inlists in our reproduction package [27].

B. Machine Learning Emulator

We trained a machine learning (ML) algorithm to predict the I-Band magnitude, M_I , the $(V - I)$ color, and the empirical uncertainties on both as a function of the MESA inputs: M , Y , Z , and μ_{12} . To emulate MESA's evolution and the WL conversion calculations, we used both a classifier and a regression Deep Neural Network (DNN). For both ML models we used the `Tensorflow Keras` package [40, 41].

For some choices of parameters, the resultant stellar model did not contribute to the TRGB. Some models did not reach the TRGB within the current age of the universe, and others burned helium stably in their core and exhibited a shell flash. Removing these models from the training set by hand can bias the emulator towards predicting viable models where there are none; so we instead trained a DNN classifier to predict whether a given set of parameters will contribute to the TRGB or not and assigned zero likelihood to models in the latter class when performing the MCMC. For classification purposes, we placed MESA evolution models into three categories: models that reached the TRGB, models that helium shell flashed¹, and models that did not core flash within the age of the Universe (13.77 billion years). A

¹ Models were flagged as shell flashing if the post-main-sequence helium-4 mass fraction fell below 0.9 as this implies the core has begun to burn helium stably.

small number of models failed to converge in MESA before they reached the TRGB. As their number was not sufficiently large to affect the training, we removed these models before beginning ML training and allowed the ML algorithm to fill in the holes in the parameter space.

ML classification algorithms perform best when the training data is relatively proportional between the respective classes. For our data, this was not the case. To account for this, we resampled the training data using the Synthetic Minority Oversampling Technique (SMOTE) [42]. SMOTE increases the sample size of undersampled areas in the parameter space without biasing the training data. The classifier was trained with the Adaptive Moment Estimation (ADAM) optimizer [43] and used categorical crossentropy loss to measure the success of the model in training. We hand-tuned the hyperparameters to optimize the classification algorithm.

We trained a DNN regressor to predict M_I , the $(V - I)$ color, and the empirical uncertainties on both as a function of M , Y , Z , and μ_{12} . The regressor was only trained on models that would not be ruled out by the classifier as older than the age of the universe or helium shell flashing. We trained the regressor using the ADAM optimizer, and used mean-squared error loss to measure the success of the regression model. Just as we did with the classifier, we hand tuned the hyperparameters to optimize the regression algorithm. We calculated the uncertainty associated with the regressor and, even though this error is sub-dominant to the WL errors, it must be accounted for. Using the testing data, distributions of error were created by taking the residual of the true and predicted values. The residuals for the ML predictions for M_I , $(V - I)$ color, and their associated empirical error are shown in Figure 1.

C. MCMC

We used an MCMC sampler to attempt to constrain μ_{12} . This compared the theoretical values of M_I^{TRGB} calculated using our ML emulator with the observations from the LMC, NGC 4258, and ω -Centauri.

We performed the MCMC analysis using the Python package `emcee` [44] with the ML stellar evolution emulator to constrain the Neutrino MDM with uncertainty. We conservatively assumed no knowledge of the input parameters and therefore used uniform priors for all of the input parameters. Our classification algorithm was used to assign a probability of zero to models which do not helium flash, or that are older than the age of the universe. Otherwise, the likelihood of a given model was calculated using the Gaussian log-likelihood function

$$P(\theta | X) = -\frac{1}{2} \left[\frac{(M_{I, \text{obs}} - M_{I, \text{corr}})^2}{\sigma^2} + \ln(2\pi\sigma^2) \right], \quad (5)$$

where $M_{I, \text{obs}}$ is the observed value for the I-band mag-

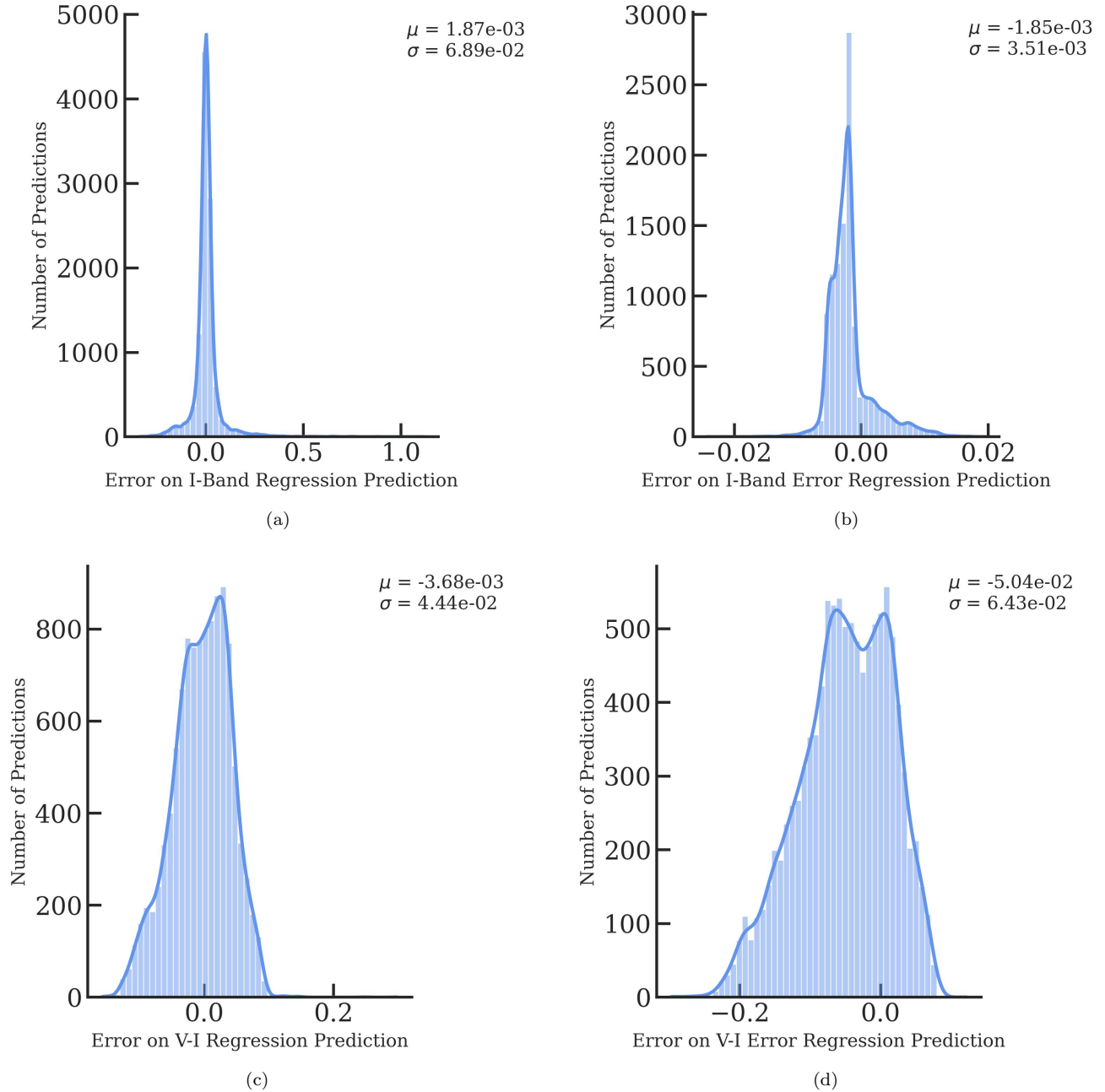


FIG. 1. Error distributions for the machine learning emulator outputs. Figure 1a shows the error on the M_I^{TRGB} prediction, Figure 1b shows the error on the M_I^{TRGB} WL error prediction, Figure 1c shows the error on the $V - I$ color prediction, and Figure 1d shows the error on the $V - I$ color error prediction. Each of these were calculated by subtracting the true value from the predicted value. μ refers to the mean and σ the standard deviation.

nitude, $M_{I, \text{corr}}$ is the color corrected ML prediction for the I-band magnitude given the input parameters (the color corrections for each system are given in Table I). In Equation (5), σ^2 is given by,

$$\sigma^2 = \sigma_{\text{obs}}^2 + \sigma_C^2, \quad (6)$$

where σ_{obs} is the I-band observational uncertainty and

σ_C is the error on the color-correction due to errors in the predicted M_I and $(V - I)$, which is given by,

$$\sigma_C \approx \left| \frac{\partial C}{\partial M_I} \right|^2 \sigma_I^2 + \left| \frac{\partial C}{\partial (V - I)} \right|^2 \sigma_{(V-I)}^2 + 2 \left| \frac{\partial C}{\partial M_I} \right| \left| \frac{\partial C}{\partial (V - I)} \right| \sigma_I \sigma_{(V-I)} \rho_{M_I(V-I)}, \quad (7)$$

where C is the corresponding color-correction, M_I is the I-band magnitude, $(V - I)$ is the $V - I$ color, σ_I is the predicted WL error on M_I , and $\sigma_{(V-I)}$ is the predicted WL error on the $V - I$ color.

To account for the uncertainties in the ML regression algorithms predictions' for the M_I , $(V - I)$, and corresponding uncertainties we use a similar approach to [45]. We added a randomly sampled value from each of the ML error distributions in Figure 1 to the predicted WL error from Equation 7. We did not account for the error on the ML classifier because it was insignificant compared to the error on the regression algorithm. The uncertainty was dominated by the WL calibration and the degeneracies, not the ML algorithm. Even so, propagating the error in the ML allowed us to completely characterize the uncertainties on the neutrino MDM constraint.

We determined that the MCMC converged if the autocorrelation time was less than 1% the length of the chain and has changed by less than 1% over the last 5,000 steps. Using this method, we consistently found that the MCMC converged in less than 200,000 steps but we allowed it to continue for 500,000 steps as a precaution, and to confirm that the walker is no longer influenced by its starting location. We discarded half the samples as burn-in. We performed our analysis on the three² calibrations of M_I^{TRGB} studied by [14] given in Table I.

III. RESULTS

A. MESA Output

Results from the grid exemplifying the relationship between M_I^{TRGB} and M , Y , Z , and μ_{12} are shown in Figure 2. As shown in Figure 2a, increasing the stellar mass results in a dimmer M_I^{TRGB} . At this stage of stellar evolution, increasing the stellar mass primarily adds more mass to the envelope, leaving the core mass relatively unchanged. This increases the opacity, resulting in a dimmer M_I^{TRGB} . Figure 2b shows that the helium abundance has only a minor effect on the brightness of the TRGB. Figure 2c shows that the I-band magnitude has a peak brightness at $Z \approx 10^{-3}$. This mirrors the relationship between the bolometric correction in this band and effective temperature. The maximum amount of light is emitted into the I-band at $T_{\text{eff}} \approx 4800\text{K}$, which, for our model parameters, occurs at $Z \approx 10^{-3}$. Finally, Figure 2d shows that, as expected and explained in detail in §I, the brightness of the tip increases with μ_{12} .

² Reference [14] studied a second LMC calibration reported by [46]. Unfortunately, the color-correction is only reported over a narrow range of $(V - I)$. Many of our models have $(V - I)$ outside this range, so we are unable to use this calibration. There is no reason to expect that our conclusions would change were a complete color-correction available.

B. Machine Learning

After training the machine learning classifier with the grid to eliminate stars that helium shell flash or are older than the age of the universe, we found an accuracy of 99.6% and a categorical crossentropy loss of 9.0×10^{-3} . Our DNN Regressor predicts M_I , $(V - I)$ color, and both WL errors with a mean squared error loss of 1.4×10^{-4} . The residuals for the regression algorithm are shown in Figure 1. The mean and standard deviation of these distributions are 1-2 orders of magnitude smaller than, and thus subdominant to, the WL and empirical uncertainties, which are on the order of 0.1 dex. The accuracy of these ML algorithms are comparable to those in [9, 10].

C. MCMC Analysis

The results from the MCMC analysis using the calibrated M_I^{TRGB} in ω -Centauri reported by [49] are shown in Figure 3. Results of the MCMC using M_I^{TRGB} calibrations of in NGC 4258 [48] and the LMC [47] are shown in Appendix A. After characterizing the uncertainties in M , Y , and Z , we find that it is possible for the value of μ_{12} to fall anywhere within our parameter space because the posterior of μ_{12} is nearly flat across the entire range. This implies that the region of parameter space $\mu_{12} \leq 6$ is unconstrained. This is explained by Figure 2c, as μ_{12} increases, more models across a wider range of Z and M fall within 1σ of the observed M_I^{TRGB} .

IV. DISCUSSION

In this section we discuss the implications of our results, suggest further applications of our method, and highlight potential caveats and limitations of our study.

A. Discussion of Our Results

The results of our MCMC are summarized in Figure 3. We find a broad marginalized posterior on μ_{12} spread across the entire parameter space. We therefore conclude that the region $\mu_{12} \leq 6$ is unconstrained when the degeneracies across parameter space are accounted for. Previous works (e.g., [14]) that do not simultaneously vary the stellar input physics with the new physics parameters find that the region $\mu_{12} < 1.2$ is excluded. Our work highlights the importance of fully accounting for stellar uncertainties when using stars as novel probes of physics beyond the Standard Model.

We further remark that the region $\mu_{12} > 6$ is not excluded by our analysis but, rather, we are unable to explore this region since our grid does not extend to higher values. Given our results, and the fact that we fixed several input physics parameters that are known to have

Target	M_I^{TRGB} Calibration [mag]	Color Correction	Reference
LMC	-3.958 ± 0.046	$0.091[(V - I) - 1.5]^2 - 0.007[(V - I) - 1.5]$	[47]
NGC 4258	-4.027 ± 0.055	$0.091[(V - I) - 1.5]^2 - 0.007[(V - I) - 1.5]$	[48]
ω -Centauri	-3.96 ± 0.05	$-0.046(V - I) + 0.08(V - I)^2$	[49]

TABLE I. Empirical M_I^{TRGB} calibrations used in this work.

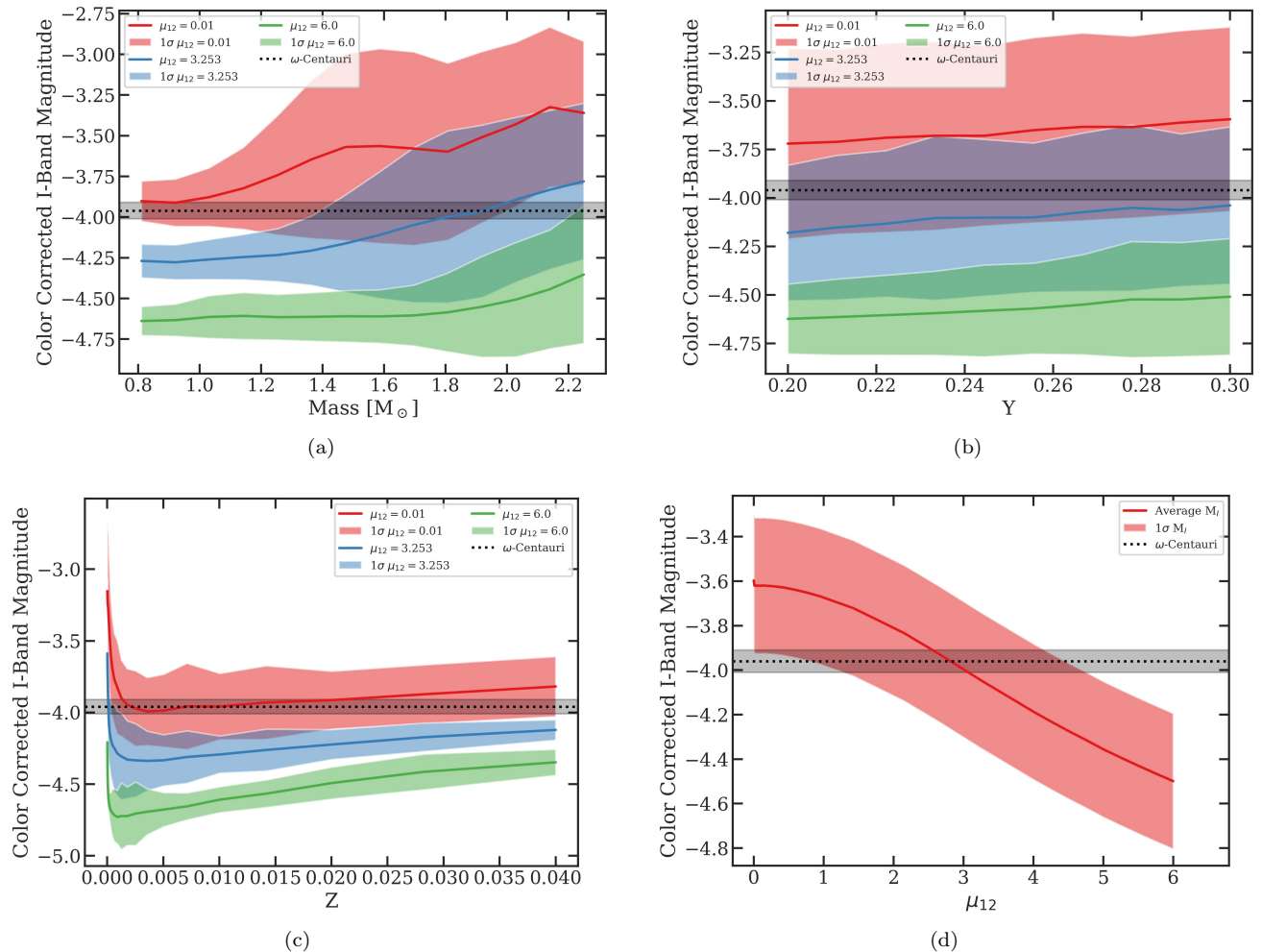


FIG. 2. I-Band magnitude as a function of each input parameter. Figures 2a, 2b, and 2c have three different values of μ_{12} as shown in the legend. The grey shaded region represents an observed value of M_I^{TRGB} calibrated ω -Centauri [49]. Each point is an average across a bin of the input parameter and each error bar represents the standard deviation in that bin.

large uncertainties, it is likely that large regions of parameter space with $\mu_{12} > 6$ are viable once stellar uncertainties are accounted for.

The opening of the parameter space has important implications for both stellar and terrestrial searches for a non-negligible neutrino magnetic dipole moment. As regards stellar probes, it is possible that a large neutrino MDM could be detected using other astrophysical objects provided that degeneracies and uncertainties with stellar physics are accounted for in a similar manner to this work. As regards to terrestrial searches, the region

of parameter space we have opened is accessible to dark matter direct detection chambers e.g., XENONnT [50], raising the possibility that these experiments could detect a non-negligible neutrino MDM.

B. Comparison with Previous Works

It is instructive to compare our results with others in the literature. A previous work [10] (authored by two of us) used a similar method to reanalyse bounds on the

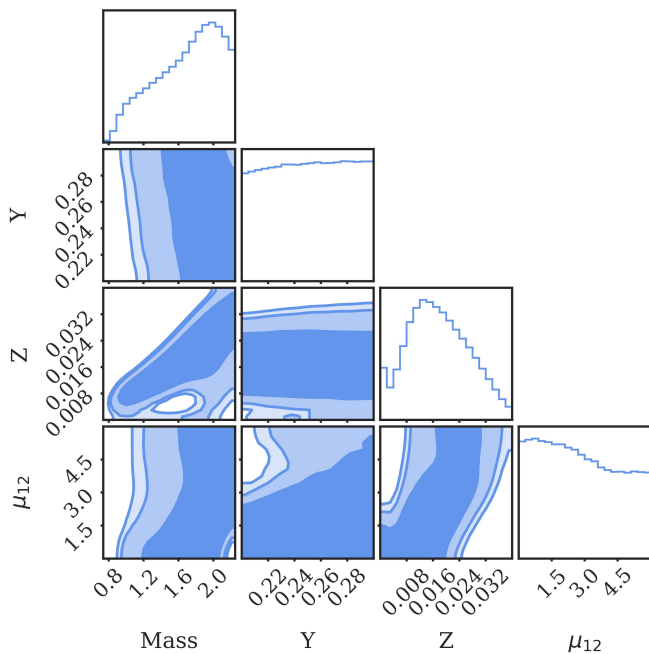


FIG. 3. Corner plot showing the results of the MCMC analysis from comparison with the M_I^{TRGB} calibration in ω -Centauri [49]. In the 2D histograms, each contour is a two dimensional confidence level with the smallest contour being 68% and increasing in size to 90% and 95%. The 1D histograms show the marginalized posterior for each input parameter.

axion-electron coupling, α_{26} . That work found similar results — namely that a large region of the axion-electron coupling parameter space is unconstrained once stellar degeneracies and uncertainties are accounted for — but there are differences in the final 2D probability distributions. In this work, we found that high μ_{12} prefers high masses $M \sim 2M_{\odot}$ and intermediate metallicities $0.008 < Z < 0.02$. In contrast, [10] found that intermediate masses $M \sim 1.2M_{\odot}$ and $Z > 0.03$ are preferred at high α_{26} . Such high metallicities may be unrealistic in light of other observations of the TRGB host objects we study.

We investigated the cause of this difference and found that it can be attributed to the difference in mixing lengths adopted by the two works. We simulated a grid of models with $\alpha_{MLT} = 1.8$ (as adopted by [10]) and $\mu_{12} = 0, 6$. In both cases we found a difference in the trend across parameter space between the two mixing lengths. In particular, we found that with $\alpha_{MLT} = 1.8$, there were a large number of $\mu_{12} = 6$ models at intermediate mass and high metallicity that were compatible with the M_I^{TRGB} calibration, consistent with the results of [10]. In contrast, Figure 2 reveals that when $\alpha_{MLT} = 2.0$ the largest density of compatible models occurs for high masses and intermediate metallicities. Our investigation demonstrates that the conclusions of [10] are not reliant upon the systems studied having super-solar metallicity. Indeed, had the mixing length been si-

multaneously varied with M , Y , and Z reference [10] would have found that a large region of parameter space with high mixing length, high mass, and intermediate metallicity — similar to the region we found in this work — is compatible with the data.

Our second comparison is with the results of [14], who report the most stringent bound $\mu_{\nu} < 1.2 \times 10^{-12} \mu_B$ at the 95% confidence level using the calibrated M_I^{TRGB} in ω -Centauri. As discussed at length in [10], the bound obtained by [14] is the result of varying stellar parameters over an extremely narrow region of parameter space that is motivated by observations of the globular cluster M5. In the language of our methodology, this corresponds to placing tight priors on the allowed range of stellar parameters. This bound is heavily-reliant upon the assumptions about M5 being valid e.g., that it is close to 13.8 Gyr old; that the measurements informing the choice of priors have their errors accurately assessed — in some cases there are competing measurements that are discrepant with one another; and that the model for M5 is a good model for the systems considered by [14]. In light of these uncertainties, we advocate for our data-driven approach, although we note that if one could use similar methods to ours to assess the errors on the measurements above then it is possible that bounds could be placed provided said errors are sufficiently small.

C. Application to Other Stellar Probes of the Neutrino Magnetic Dipole Moment

An important application of our method is to reevaluate other stellar bounds on the neutrino MDM. There are no astrophysical probes of fundamental physics that are free from degeneracies and uncertainties, and our work has highlighted the importance of accounting for these when placing bounds. In the case of the neutrino MDM, our methodology could be used to revisit bounds coming from the Sun [51] and the white dwarf luminosity function [52]. With the TRGB bounds now allowing values of $\mu_{12} \leq 6$, the latter test, which yields $\mu_{12} < 5$, is presently the most constraining.

D. Limitations of Our Study

Our work is subject to some limitations that we now discuss. First, as a result of limited computation time, we do not vary all possible input parameters such as mixing length, radiative opacity, conductive opacity, nuclear reaction rates, neutrino loss rate, mass loss, and others listed in [21, 22]. As a result, our uncertainties are most likely underestimated. In future work, this could be improved upon by varying more parameters in a larger grid, increasing the number of stellar simulations. This would be computationally expensive. For example, if we were to vary 10 stellar parameters the grid would take ~ 2 billion CPU years to complete. Our grid with four param-

ters varying completed in ~ 23 CPU years. More efficient sampling methods such as Latin hypercube sampling or active learning [53] could speed this up dramatically. Another novel challenge in this endeavor is the longer convergence times for random walk MCMC algorithms in higher-dimensional parameter spaces. This could be overcome by using Hamiltonian MCMC (HMCMC). A major advantage of using DNNs is that they are differentiable, which is necessary for HMCMC. We remark that increasing further sources of uncertainty can only strengthen the conclusions of this work, but doing so would allow one to determine the boundary of the region of parameter space excluded by TRGB measurements.

A second limitation is that we define the TRGB using a single stellar evolution model. This is tantamount to assuming that the TRGB I-band magnitude is due to the brightest star. The goal of this work is to compare with other works that made this identical assumption (e.g. [37, 54]). Observationally, M_I^{TRGB} is calibrated using edge-finding techniques applied to the entire color-magnitude diagram [20], which includes a multitude of stars with varying stellar parameters and a complex star formation history. Going beyond the single-star approximation would enable a more consistent comparison with observation. One could accomplish this by first using our ML emulator to create synthetic color-magnitude diagrams by simulating a population of stars with parameters drawn from some distribution, and then applying the same edge-finding techniques to these to obtain a more realistic prediction for M_I^{TRGB} . Using edge-finding techniques would increase the uncertainties and, as a consequence, increase the unconstrained region because there would be a larger spread in the simulated values of M_I^{TRGB} . This makes an interesting topic for future work.

A final limitation is that our method includes statistical uncertainties but not systematic uncertainties. For example, we used a single stellar structure code with certain discrete choices e.g., elemental abundances, numerical solver, atmosphere model, etc. Using a different code may give different results. Similarly, important physics not captured by MESA e.g., three-dimensional processes could be another source of systematics. Finally, we used the bolometric corrections of Worthey & Lee [35] but other choices e.g., MARCS [55] or PHOENIX [56] may give different predictions for M_I^{TRGB} and its empirical uncertainty. It would be interesting to repeat our work using different stellar structure codes and different bolometric corrections and compare the results.

V. CONCLUSIONS

In this work we utilized a novel methodology to constrain the neutrino magnetic dipole moment (MDM) using empirical calibrations of the tip of the red giant branch (TRGB) I-band magnitude (M_I^{TRGB}) that fully accounts for uncertainties and degeneracies due to stellar input physics. We first simulated 146,250 MESA mod-

els, varying the stellar mass (M), helium abundance (Y), metallicity (Z), and the reduced neutrino MDM ($\mu_{12} = \mu_\nu \times 10^{-12} \mu_B$). We then used the bolometric correction code from Worthey & Lee [35] to calculate the I-Band magnitude of the TRGB for each model. Next, we trained a machine learning algorithm to predict M_I^{TRGB} and its associated uncertainty given values of the four input parameters. Finally, we used our ML emulator to make theoretical predictions for M_I^{TRGB} in an MCMC analysis that compared them with empirical calibrations to constrain the neutrino MDM. We found that once stellar uncertainties are fully accounted for, observations of the TRGB do not place any constraints on the neutrino MDM when $\mu_{12} \leq 6$. Furthermore, given the broad and flat posterior we found, it is likely that larger values are equally unconstrained, although our grid does not extend to larger values to confirm this. Our study has opened up a large region of parameter space that was previously believed to be excluded. This region is accessible to planned terrestrial dark matter direct detection chambers. It is highly likely that the bounds on the neutrino MDM from other stellar probes will be similarly weakened once degeneracies are fully accounted for. The methodology we have utilized can be applied to these tests in a straightforward manner, and doing so is of paramount importance for determining the viable parameter space of theories beyond the Standard Model.

VI. SOFTWARE

MESA version 12778, MESASDK version 20.3.2, python version 3.8, NumPy version 1.22.3 [57], Pandas version 1.4.3 [58, 59], Matplotlib version 3.5.1 [60], Seaborn version 0.11.2 [61], Tensorflow version 2.4.1 [40, 41], corner version 2.2.1 [62], emcee version 3.1.2 [44].

VII. ACKNOWLEDGEMENTS

We thank Adrian Ayala, Aaron Dotter, Robert Farmer, Frank Timmes, and the wider MESA community for answering our MESA-related questions. We are grateful for conversations with Eric J. Baxter, Djuna Croon, Samuel D. McDermott, Harry Desmond, Marco Gatti, Dan Hey, Jason Kumar, Danny Marfatia, Marco Raveri, David Rubin, Xerxes Tata, and Guy Worthey. We are especially thankful to David Schanzenbach for his assistance with using the University of Hawai‘i MANA supercomputer.

NF acknowledges support from Research Experience for Undergraduate program at the Institute for Astronomy, University of Hawai‘i-Manoa funded through NSF grant #2050710. NF would like to thank the Institute for Astronomy for their hospitality during the course of this project. To run our stellar evolution simulations and much of our analysis we utilized the University of Hawai‘i’s high-performance supercomputer MANA. The

technical support and advanced computing resources from University of Hawaii Information Technology Ser-

vices – Cyberinfrastructure, funded in part by the National Science Foundation MRI award #1920304, are gratefully acknowledged.

-
- [1] G. G. Raffelt, *Stars as laboratories for fundamental physics : the astrophysics of neutrinos, axions, and other weakly interacting particles* (1996).
- [2] G. G. Raffelt, *Astrophysics probes of particle physics*, PhR **333**, 593 (2000).
- [3] D. J. E. Marsh, Axions and ALPs: a very short introduction, arXiv e-prints , arXiv:1712.03018 (2017), arXiv:1712.03018 [hep-ph].
- [4] L. Di Luzio, M. Fedele, M. Giannotti, F. Mescia, and E. Nardi, Solar Axions Cannot Explain the XENON1T Excess, PhRvL **125**, 131804 (2020), arXiv:2006.12487 [hep-ph].
- [5] F. Chadha-Day, J. Ellis, and D. J. E. Marsh, Axion dark matter: What is it and why now?, Science Advances **8**, eabj3618 (2022), arXiv:2105.01406 [hep-ph].
- [6] Fabbrichesi, Marco and Gabrielli, Emidio and Lanfranchi, Gaia, *The Physics of the Dark Photon* (Springer Cham, 2021).
- [7] C. Brogini, C. Giunti, and A. Studenikin, Electromagnetic Properties of Neutrinos, arXiv e-prints , arXiv:1207.3980 (2012), arXiv:1207.3980 [hep-ph].
- [8] S. Alexander, Status and perspectives of neutrino magnetic moments, Journal of Physics: Conference Series **718**, 062076 (2016).
- [9] M. Dennis and J. Sakstein, Machine Learning the Tip of the Red Giant Branch, (2023), arXiv:2303.12069 [astro-ph.GA].
- [10] M. T. Dennis and J. Sakstein, Tip of the Red Giant Branch Bounds on the Axion-Electron Coupling Revisited, (2023), arXiv:2305.03113 [hep-ph].
- [11] R. N. Mohapatra and P. B. Pal, *Massive neutrinos in physics and astrophysics*, Vol. 41 (1991).
- [12] K. Winter, *Neutrino physics* (1991).
- [13] A. Aboubrahim, T. Ibrahim, A. Itani, and P. Nath, Large neutrino magnetic dipole moments in MSSM extensions, PhRvD **89**, 055009 (2014), arXiv:1312.2505 [hep-ph].
- [14] F. Capozzi and G. Raffelt, Axion and neutrino bounds improved with new calibrations of the tip of the red-giant branch using geometric distance determinations, PhRvD **102**, 083007 (2020), arXiv:2007.03694 [astro-ph.SR].
- [15] H. Shapley, *Star Clusters*, Vol. 2 (1930).
- [16] W. Baade, The Resolution of Messier 32, NGC 205, and the Central Region of the Andromeda Nebula., ApJ **100**, 137 (1944).
- [17] G. S. Da Costa and T. E. Armandroff, Standard Globular Cluster Giant Branches in the (M(I), (V - I)o) Plane, AJ **100**, 162 (1990).
- [18] W. L. Freedman and B. F. Madore, The Hubble Constant, ARA&A **48**, 673 (2010), arXiv:1004.1856 [astro-ph.CO].
- [19] W. L. Freedman and B. F. Madore, Astrophysical Distance Scale. II. Application of the JAGB Method: A Nearby Galaxy Sample, ApJ **899**, 67 (2020), arXiv:2005.10793 [astro-ph.GA].
- [20] M. G. Lee, W. L. Freedman, and B. F. Madore, The Tip of the Red Giant Branch as a Distance Indicator for Resolved Galaxies, ApJ **417**, 553 (1993).
- [21] A. Serenelli, A. Weiss, S. Cassisi, M. Salaris, and A. Pietrinferni, The brightness of the red giant branch tip. Theoretical framework, a set of reference models, and predicted observables, A&A **606**, A33 (2017), arXiv:1706.09910 [astro-ph.SR].
- [22] I. D. Saltas and E. Tognelli, New calibrated models for the TRGB luminosity and a thorough analysis of theoretical uncertainties, arXiv e-prints , arXiv:2203.02499 (2022), arXiv:2203.02499 [astro-ph.SR].
- [23] A. Heger, A. Friedland, M. Giannotti, and V. Cirigliano, The Impact of Neutrino Magnetic Moments on the Evolution of Massive Stars, ApJ **696**, 608 (2009), arXiv:0809.4703 [astro-ph].
- [24] G. G. Raffelt, Core Mass at the Helium Flash from Observations and a New Bound on Neutrino Electromagnetic Properties, ApJ **365**, 559 (1990).
- [25] G. Raffelt and A. Weiss, Non-standard neutrino interactions and the evolution of red giants, A&A **264**, 536 (1992).
- [26] V. Castellani and S. degl'Innocenti, Stellar Evolution as a Probe of Neutrino Properties, ApJ **402**, 574 (1993).
- [27] N. Franz, M. T. Dennis, and J. Sakstein, Tip of the Red Giant Branch Bounds on the Neutrino Magnetic Dipole Moment Revisited, 10.5281/zenodo.8173321 (2023).
- [28] B. Paxton, L. Bildsten, A. Dotter, F. Herwig, P. Lesaffre, and F. Timmes, Modules for Experiments in Stellar Astrophysics (MESA), ApJS **192**, 3 (2011), arXiv:1009.1622 [astro-ph.SR].
- [29] B. Paxton, M. Cantiello, P. Arras, L. Bildsten, E. F. Brown, A. Dotter, C. Mankovich, M. H. Montgomery, D. Stello, F. X. Timmes, and R. Townsend, Modules for Experiments in Stellar Astrophysics (MESA): Planets, Oscillations, Rotation, and Massive Stars, ApJS **208**, 4 (2013), arXiv:1301.0319 [astro-ph.SR].
- [30] B. Paxton, P. Marchant, J. Schwab, E. B. Bauer, L. Bildsten, M. Cantiello, L. Dessart, R. Farmer, H. Hu, N. Langer, R. H. D. Townsend, D. M. Townsley, and F. X. Timmes, Modules for Experiments in Stellar Astrophysics (MESA): Binaries, Pulsations, and Explosions, ApJS **220**, 15 (2015), arXiv:1506.03146 [astro-ph.SR].
- [31] B. Paxton, J. Schwab, E. B. Bauer, L. Bildsten, S. Blinnikov, P. Duffell, R. Farmer, J. A. Goldberg, P. Marchant, E. Sorokina, A. Thoul, R. H. D. Townsend, and F. X. Timmes, Modules for Experiments in Stellar Astrophysics (MESA): Convective Boundaries, Element Diffusion, and Massive Star Explosions, ApJS **234**, 34 (2018), arXiv:1710.08424 [astro-ph.SR].
- [32] B. Paxton, R. Smolec, J. Schwab, A. Gautschi, L. Bildsten, M. Cantiello, A. Dotter, R. Farmer, J. A. Goldberg, A. S. Jermyn, S. M. Kanbur, P. Marchant, A. Thoul, R. H. D. Townsend, W. M. Wolf, M. Zhang, and F. X. Timmes, Modules for Experiments in Stellar Astrophysics (MESA): Pulsating Variable Stars, Rotation, Convective Boundaries, and Energy Conservation, ApJS **243**, 10 (2019), arXiv:1903.01426 [astro-ph.SR].

- [33] A. S. Jermyn, E. B. Bauer, J. Schwab, R. Farmer, W. H. Ball, E. P. Bellinger, A. Dotter, M. Joyce, P. Marchant, J. S. G. Mombarg, W. M. Wolf, T. L. S. Wong, G. C. Cinquegrana, E. Farrell, R. Smolec, A. Thoul, M. Cantiello, F. Herwig, O. Toloza, L. Bildsten, R. H. D. Townsend, and F. X. Timmes, Modules for Experiments in Stellar Astrophysics (MESA): Time-Dependent Convection, Energy Conservation, Automatic Differentiation, and Infrastructure, arXiv e-prints , arXiv:2208.03651 (2022), arXiv:2208.03651 [astro-ph.SR].
- [34] M. Haft, G. Raffelt, and A. Weiss, Standard and Non-standard Plasma Neutrino Emission Revisited, *ApJ* **425**, 222 (1994), arXiv:astro-ph/9309014 [astro-ph].
- [35] G. Worthey and H.-c. Lee, An Empirical UBV RI JHK Color-Temperature Calibration for Stars, *ApJS* **193**, 1 (2011), arXiv:astro-ph/0604590 [astro-ph].
- [36] N. Viaux, M. Catelan, P. B. Stetson, G. G. Raffelt, J. Reondo, A. A. R. Valcarce, and A. Weiss, Particle-physics constraints from the globular cluster M5: neutrino dipole moments, *A&A* **558**, A12 (2013), arXiv:1308.4627 [astro-ph.SR].
- [37] F. Capozzi and G. Raffelt, Axion and neutrino bounds improved with new calibrations of the tip of the red-giant branch using geometric distance determinations, *PhRvD* **102**, 083007 (2020), arXiv:2007.03694 [astro-ph.SR].
- [38] R. Kippenhahn, A. Weigert, and A. Weiss, *Stellar Structure and Evolution* (2013).
- [39] M. Dennis and J. Sakstein, Machine Learning the Tip of the Red Giant Branch, arXiv e-prints , arXiv:2303.12069 (2023), arXiv:2303.12069 [astro-ph.GA].
- [40] M. Abadi, A. Agarwal, P. Barham, E. Brevdo, Z. Chen, C. Citro, G. S. Corrado, A. Davis, J. Dean, M. Devin, S. Ghemawat, I. Goodfellow, A. Harp, G. Irving, M. Isard, Y. Jia, R. Jozefowicz, L. Kaiser, M. Kudlur, J. Levenberg, D. Mané, R. Monga, S. Moore, D. Murray, C. Olah, M. Schuster, J. Shlens, B. Steiner, I. Sutskever, K. Talwar, P. Tucker, V. Vanhoucke, V. Vasudevan, F. Viégas, O. Vinyals, P. Warden, M. Wattenberg, M. Wicke, Y. Yu, and X. Zheng, TensorFlow: Large-scale machine learning on heterogeneous systems (2015), software available from tensorflow.org.
- [41] F. Chollet *et al.*, Keras, <https://keras.io> (2015).
- [42] N. V. Chawla, K. W. Bowyer, L. O. Hall, and W. P. Kegelmeyer, SMOTE: Synthetic Minority Over-sampling Technique, *Journal of artificial intelligence research* , arXiv:1106.1813 (2002), arXiv:1106.1813 [cs.AI].
- [43] D. P. Kingma and J. Ba, Adam: A Method for Stochastic Optimization, arXiv e-prints , arXiv:1412.6980 (2014), arXiv:1412.6980 [cs.LG].
- [44] D. Foreman-Mackey, D. W. Hogg, D. Lang, and J. Goodman, emcee: the mcmc hammer, *Publications of the Astronomical Society of the Pacific* **125**, 306 (2013).
- [45] T. McClintock, T. N. Varga, D. Gruen, E. Rozo, E. S. Rykoff, T. Shin, P. Melchior, J. DeRose, S. Seitz, J. P. Dietrich, E. Sheldon, Y. Zhang, A. von der Linden, T. Jeltema, A. B. Mantz, A. K. Romer, S. Allen, M. R. Becker, A. Bermeo, S. Bhargava, M. Costanzi, S. Everett, A. Farahi, N. Hamaus, W. G. Hartley, D. L. Hollowood, B. Hoyle, H. Israel, P. Li, N. MacCrann, G. Morris, A. Palmese, A. A. Plazas, G. Pollina, M. M. Rau, M. Simet, M. Soares-Santos, M. A. Troxel, C. Vergara Cervantes, R. H. Wechsler, J. Zuntz, T. M. C. Abbott, F. B. Abdalla, S. Allam, J. Annis, S. Avila, S. L. Bridle, D. Brooks, D. L. Burke, A. Carnero Rosell, M. Carrasco Kind, J. Carretero, F. J. Castander, M. Crocce, C. E. Cunha, C. B. D’Andrea, L. N. da Costa, C. Davis, J. De Vicente, H. T. Diehl, P. Doel, A. Drlica-Wagner, A. E. Evrard, B. Flaugher, P. Fosalba, J. Frieman, J. García-Bellido, E. Gaztanaga, D. W. Gerdes, T. Giannantonio, R. A. Gruendl, G. Gutierrez, K. Honscheid, D. J. James, D. Kirk, E. Krause, K. Kuehn, O. Lahav, T. S. Li, M. Lima, M. March, J. L. Marshall, F. Menanteau, R. Miquel, J. J. Mohr, B. Nord, R. L. C. Ogando, A. Roodman, E. Sanchez, V. Scarpine, R. Schindler, I. Sevilla-Noarbe, M. Smith, R. C. Smith, F. Sobreira, E. Suchyta, M. E. C. Swanson, G. Tarle, D. L. Tucker, V. Vikram, A. R. Walker, J. Weller, and DES Collaboration, Dark Energy Survey Year 1 results: weak lensing mass calibration of redMaPPer galaxy clusters, *MNRAS* **482**, 1352 (2019), arXiv:1805.00039 [astro-ph.CO].
- [46] W. L. Freedman, B. F. Madore, T. Hoyt, I. S. Jang, R. Beaton, M. G. Lee, A. Monson, J. Neeley, and J. Rich, Calibration of the Tip of the Red Giant Branch, *ApJ* **891**, 57 (2020), arXiv:2002.01550 [astro-ph.GA].
- [47] W. Yuan, A. G. Riess, L. M. Macri, S. Casertano, and D. M. Scolnic, Consistent Calibration of the Tip of the Red Giant Branch in the Large Magellanic Cloud on the Hubble Space Telescope Photometric System and a Redetermination of the Hubble Constant, *ApJ* **886**, 61 (2019), arXiv:1908.00993 [astro-ph.GA].
- [48] I. S. Jang and M. G. Lee, The Tip of the Red Giant Branch Distances to Type Ia Supernova Host Galaxies. IV. Color Dependence and Zero-point Calibration, *ApJ* **835**, 28 (2017), arXiv:1611.05040 [astro-ph.GA].
- [49] M. Bellazzini, F. R. Ferraro, and E. Pancino, A Step toward the Calibration of the Red Giant Branch Tip as a Standard Candle, *ApJ* **556**, 635 (2001), arXiv:astro-ph/0104114 [astro-ph].
- [50] E. Aprile, J. Aalbers, F. Agostini, M. Alfonsi, L. Althueser, F. D. Amaro, V. C. Antochi, E. Angelino, J. R. Angevaere, F. Arneodo, D. Barge, L. Baudis, B. Bauermeister, L. Bellagamba, M. L. Benabderrahmane, T. Berger, A. Brown, E. Brown, S. Bruenner, G. Bruno, R. Budnik, C. Capelli, J. M. R. Cardoso, D. Cichon, B. Cimmino, M. Clark, D. Coderre, A. P. Colijn, J. Conrad, J. P. Cussonneau, M. P. Decowski, A. Depoian, P. di Gangi, A. di Giovanni, R. di Stefano, S. Diglio, A. Elykov, G. Eurin, A. D. Ferella, W. Fulgione, P. Gaemers, R. Gaior, M. Galloway, F. Gao, L. Grandi, C. Hasterok, C. Hils, K. Hiraide, L. Hoetsch, J. Howlett, M. Iacovacci, Y. Itow, F. Joerg, N. Kato, S. Kazama, M. Kobayashi, G. Koltman, A. Kopec, H. Landsman, R. F. Lang, L. Levinson, Q. Lin, S. Lindemann, M. Lindner, F. Lombardi, J. Long, J. A. M. Lopes, E. López Fune, C. Macolino, J. Mahlstedt, A. Mancuso, L. Manenti, A. Manfredini, F. Marignetti, T. Marrodán Undagoitia, K. Martens, J. Masbou, D. Masson, S. Mastroianni, M. Messina, K. Miuchi, K. Mizukoshi, A. Molinaro, K. Morá, S. Moriyama, Y. Mosbacher, M. Murra, J. Naganoma, K. Ni, U. Oberlack, K. Odgers, J. Palocio, B. Pelssers, R. Peres, J. Pienaar, V. Pizzella, G. Plante, J. Qin, H. Qiu, D. Ramírez García, S. Reichard, A. Rochetti, N. Rupp, J. M. F. Dos Santos, G. Sartorelli, N. Šarčević, M. Scheibelhut, J. Schreiner, D. Schulte, M. Schumann, L. Scotto Lavina, M. Selvi, F. Semeria, P. Shagin, E. Shockley, M. Silva, H. Simgen, A. Takeda, C. Therreau, D. Thers, F. Toschi, G. Trincherro, C. Tunnel, M. Vargas, G. Volta, H. Wang, Y. Wei, C. Wein-

- heimer, M. Weiss, D. Wenz, C. Wittweg, Z. Xu, M. Yamashita, J. Ye, G. Zavattini, Y. Zhang, T. Zhu, J. P. Zopounidis, and X. Xenon Collaboration, Mougeot, Excess electronic recoil events in XENON1T, *PhRvD* **102**, 072004 (2020), arXiv:2006.09721 [hep-ex].
- [51] M. Agostini *et al.* (Borexino), Limiting neutrino magnetic moments with Borexino Phase-II solar neutrino data, *Phys. Rev. D* **96**, 091103 (2017), arXiv:1707.09355 [hep-ex].
- [52] M. M. Miller Bertolami, Limits on the neutrino magnetic dipole moment from the luminosity function of hot white dwarfs, *A&A* **562**, A123 (2014), arXiv:1407.1404 [hep-ph].
- [53] K. Akira Rocha, J. J. Andrews, C. P. L. Berry, Z. Doctor, A. K. Katsaggelos, J. G. Serra Pérez, P. Marchant, V. Kalogera, S. Coughlin, S. S. Bavera, A. Dotter, T. Fragos, K. Kowlakas, D. Misra, Z. Xing, and E. Zappatas, Active Learning for Computationally Efficient Distribution of Binary Evolution Simulations, arXiv e-prints, arXiv:2203.16683 (2022), arXiv:2203.16683 [astro-ph.SR].
- [54] G. Raffelt and A. Weiss, Red giant bound on the axion-electron coupling reexamined, *PhRvD* **51**, 1495 (1995), arXiv:hep-ph/9410205 [hep-ph].
- [55] B. Gustafsson, B. Edvardsson, K. Eriksson, U. G. Jørgensen, Å. Nordlund, and B. Plez, A grid of MARCS model atmospheres for late-type stars. I. Methods and general properties, *A&A* **486**, 951 (2008), arXiv:0805.0554 [astro-ph].
- [56] A. Dotter, B. Chaboyer, D. Jevremović, V. Kostov, E. Baron, and J. W. Ferguson, The Dartmouth Stellar Evolution Database, *ApJS* **178**, 89 (2008), arXiv:0804.4473 [astro-ph].
- [57] C. R. Harris, K. J. Millman, S. J. van der Walt, R. Gommers, P. Virtanen, D. Cournapeau, E. Wieser, J. Taylor, S. Berg, N. J. Smith, R. Kern, M. Picus, S. Hoyer, M. H. van Kerkwijk, M. Brett, A. Haldane, J. F. del Río, M. Wiebe, P. Peterson, P. Gérard-Marchant, K. Sheppard, T. Reddy, W. Weckesser, H. Abbasi, C. Gohlke, and T. E. Oliphant, Array programming with NumPy, *Nature* **585**, 357 (2020).
- [58] Wes McKinney, Data Structures for Statistical Computing in Python, in *Proceedings of the 9th Python in Science Conference*, edited by Stéfan van der Walt and Jarrod Millman (2010) pp. 56 – 61.
- [59] T. pandas development team, pandas-dev/pandas: Pandas (2020).
- [60] J. D. Hunter, Matplotlib: A 2d graphics environment, *Computing in Science & Engineering* **9**, 90 (2007).
- [61] M. L. Waskom, seaborn: statistical data visualization, *Journal of Open Source Software* **6**, 3021 (2021).
- [62] D. Foreman-Mackey, corner.py: Scatterplot matrices in python, *The Journal of Open Source Software* **1**, 24 (2016).

Appendix A: Further MCMC Results

Corner plots showing the results from comparison with the M_I^{TRGB} calibrations from [47] and [48] are in Figures 4 and 5, respectively.

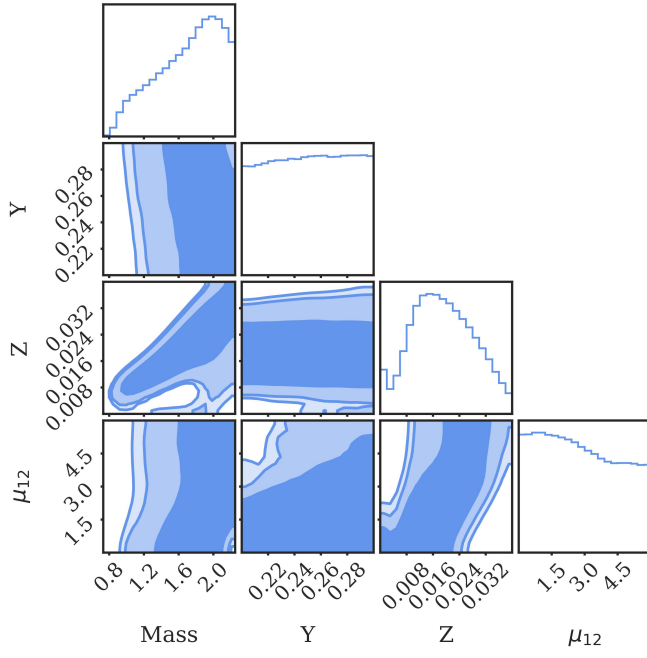


FIG. 4. Same as Figure 3 except the MCMC analysis was done with comparison to the M_I^{TRGB} calibration from [47].

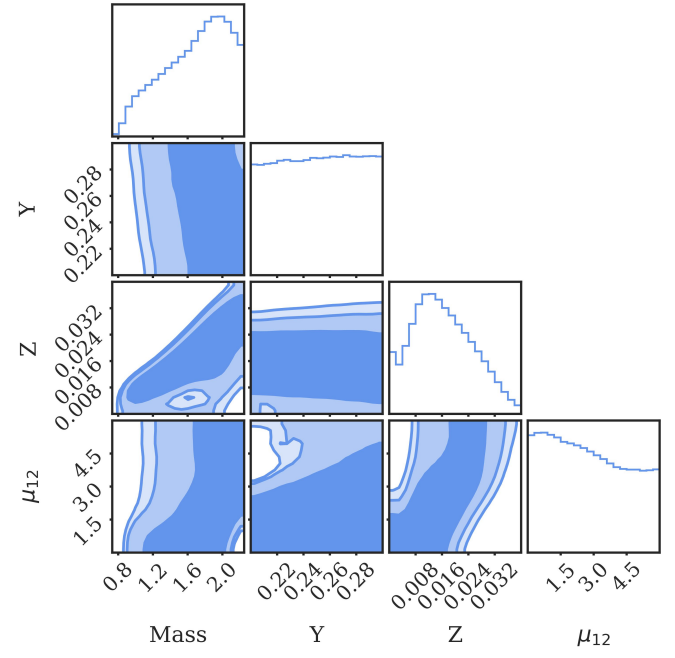


FIG. 5. Same as Figure 3 except the MCMC analysis was done with comparison to the M_I^{TRGB} calibration from [48].